

SECOND EUROPEAN ROTORCRAFT AND POWERED LIFT AIRCRAFT FORUM

Paper No. 15

C. R. Vause, F. H. Schmitz, and D. A. Boxwell  
Ames Directorate  
U.S. Army Air Mobility R&D Laboratory  
Moffett Field, California 94035, U.S.A.

September 20 - 22, 1976

Bückerburg, Federal Republic of Germany

Deutsche Gesellschaft für Luft- und Raumfahrt e.V.

Postfach 510645, D-5000 Köln, Germany

# HIGH-SPEED HELICOPTER IMPULSIVE NOISE

C. R. Vause, F. H. Schmitz, and D. A. Boxwell  
Research Scientists  
Ames Directorate  
U.S. Army Air Mobility R&D Laboratory  
Moffett Field, California 94035, U.S.A.

## 1. Abstract

Forward flight impulsive noise data from a 1/7-scale UH-1H model rotor have been gathered in an acoustically treated wind tunnel and are compared with full-scale acoustic flight-test data for the same helicopter. Good agreement between model and full-scale waveforms and peak pressure amplitudes is noted when key performance parameters are matched and the data are acoustically scaled. In-plane acoustic radiation characteristics of the model data are presented for variations in thrust, advance ratio, tip-path-plane angle, and advancing tip Mach number. The acoustic waveform exhibits changes in character as advancing tip Mach number ( $M_{AT}$ ) is increased, becoming almost discontinuous at high  $M_{AT}$ . This step increase in acoustic pressure correlates with schlieren photographs of a periodic pressure wave which radiates from the advancing rotor blade to the acoustic far field.

## 2. Introduction

When present, the most offensive and easily detectable sound a helicopter generates is "impulsive noise" - more commonly called "blade slap." Its distinctive character and high-level radiated acoustic energy often create major problems for military and civilian operations. For this reason, much effort has been spent trying to understand the aerodynamic origins and mechanisms of "impulsive noise."

One of the earliest experimental investigations of high-speed rotor noise was done by Hilton.<sup>1</sup> Working with model propellers on a static test stand, he was able to visualize shock and acoustic waves by utilizing high-speed schlieren techniques. Several other researchers<sup>2,3</sup> developed simple theories and made acoustic measurements<sup>4</sup> of high-speed propellers. The era of the jet engine, however, decreased the urgency of this research, and the field became generally dormant.

Helicopter designs, particularly in the last 10 years, have increasingly called for high main and tail rotor tip speeds in order to minimize total vehicle weight and maximize payload. With the combination of high hovering tip speeds and high forward velocities, helicopter rotors frequently operate in a compressible flow environment - not unlike the environment of the high-tip-speed propeller - giving rise to the blade slap problem. As a result, there has been a renewed interest in understanding the mechanisms which cause impulsive noise. Many theoretical investigations have been undertaken and much progress is being made in the development of mathematical models of the generation process.<sup>5-8</sup> A major difficulty in understanding and predicting rotor noise, however, is the difficulty in establishing boundary conditions on the rotor; i.e., predicting detailed aerodynamics in the unsteady three-dimensional lifting environment of the translating and rotating blade.

Experimental investigations have also helped focus attention on the aerodynamic origins of impulsive noise. Recent in-flight acoustic measurements<sup>9</sup> have shown that, for the UH-1H helicopter, there are three separable types of impulsive noise, exhibiting identifiable sounds, which can be traced to distinct aerodynamic events (Figure 1).

The first type of impulsive noise is caused by blade-vortex interaction (Figure 1, No. 1) and is dependent on wake geometry. The second and third types (Figure 1, Nos. 2 and 3) are compressibility effects that are related to high tip speeds and high forward speeds. The data<sup>9</sup> also indicate that high-speed impulsive noise cannot be heard in the cabin of the helicopter, and is the major type of in-plane noise for the UH-1H helicopter. Because helicopters generally operate at low altitudes, most surrounding land surface areas are subjected to this in-plane high-speed impulsive noise.

In this paper, the natural follow-on experiment to Reference 9 is presented. A 1/7 geometrically scaled model rotor was tested in an acoustically treated wind tunnel over many of the same operating conditions as the full-scale investigation. The major purposes of this high-tip-speed model test were to: (1) identify regimes where model testing can adequately scale the acoustic events; (2) isolate those nondimensional parameters which govern acoustic scaling; (3) explore selected parameter

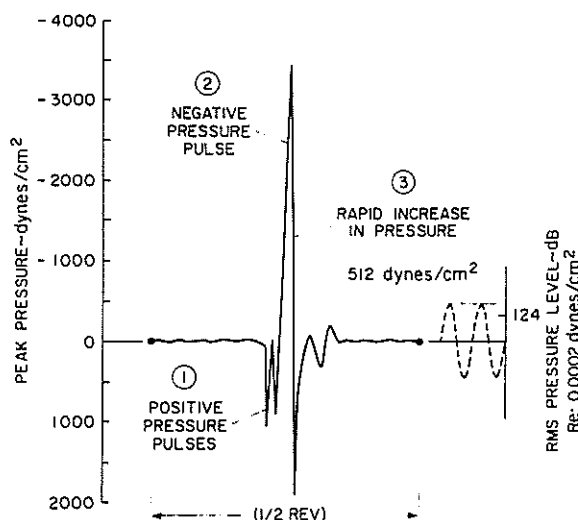


Figure 1. Composite illustration showing dominant UH-1H acoustic waveform features (Reference 9).

riations; and (4) further identify and quantify high-speed impulsive noise mechanisms in a controlled environment. Schlieren techniques were used to visualize the compressible flow near the rotor and the propagation of a radiated shock (pressure discontinuity).

### Model Scaling

The tremendous advantages of using the in-flight far-field measurement techniques of Reference 9, together with a scaled model wind-tunnel acoustic test, are illustrated in Figure 2. During the in-flight tests, the medium (air) was stationary while the helicopter and microphone were flown to maintain chosen angular and separation distances. These same angles and scaled separation distances were matched as closely as possible in the wind tunnel, where the medium (air) was moving and the microphone and rotor hub were at fixed spatial positions. Changes in full-scale descent rates cause changes in the rotor's tip-path-plane angle; these descent-rate changes were easily provided by tilting the shaft in the model experiment. Comparison of model data to full-scale measurements is one-to-one. No Doppler shift corrections had to be applied to either set of data (as would be case if the tunnel data were compared with full-scale flyby data); scaled separation distances and transmission path geometries are similar.

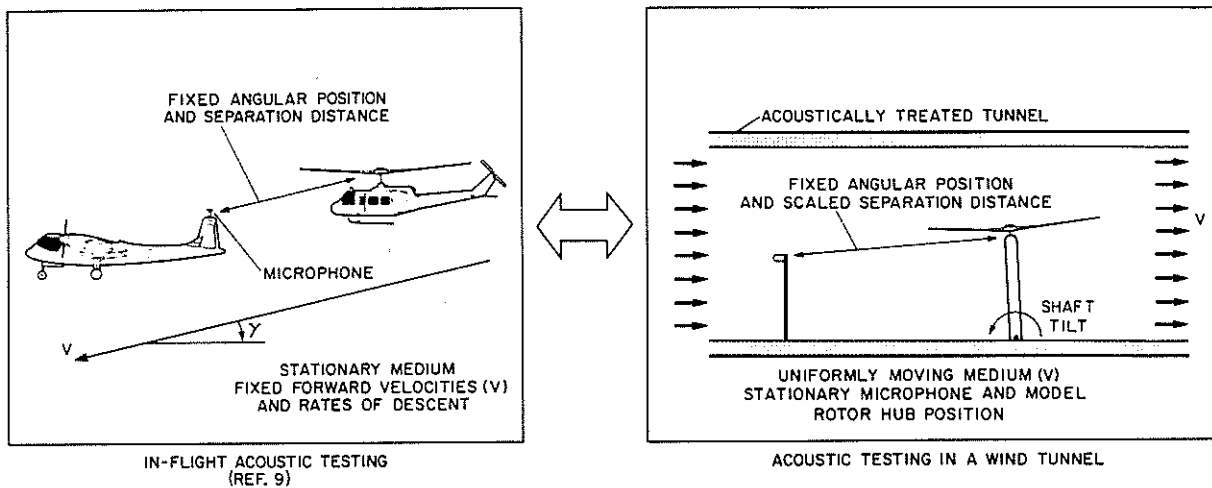


Figure 2. Schematic comparison of in-flight and wind-tunnel acoustic test procedures.

High-speed impulsive noise is thought to be governed by compressibility considerations. It was important, therefore, that the local Mach number on the model blade be scaled. To accomplish this, the scaled lift must be similar, with the same blade geometry (0012 airfoil section, rectangular planform, near  $10.9^\circ$  washout twist distribution), thrust coefficient, advance ratio, and tip-path-plane angles. If all of these variables were held constant, the model rotor was geometrically reduced by a factor of 7 while shaft rotational rate was increased by this same factor. A table comparing the important dimensional and nondimensional aerodynamic variables of the in-flight test of Reference 9 with the model wind-tunnel test is given in Appendix A. Operationally, four nondimensional variables were matched during the model testing: hover tip Mach number ( $M_H$ ); advance ratio ( $\mu$ ); thrust coefficient ( $C_T$ ); and tip-path-plane angle ( $\alpha_{TPP}$ ). By matching full-scale hover tip Mach number and advance ratio, the advancing tip Mach number ( $M_{AT}$ ) is also duplicated.

Unfortunately, not all nondimensional variables (such as Reynolds number, which affects boundary conditions on the surface of the blade) could be scaled: nor were blade structural properties scaled, since they are thought to have a secondary influence on high-tip-speed acoustic radiation.

### Acoustic Instrumentation

It has been known for some time that obtaining meaningful acoustic measurements in hard-walled wind tunnels can be quite difficult. The Ames 7- by 10-Foot Wind Tunnel is no exception.<sup>10</sup> Background noise levels, strong reverberation effects, and local flow noise — all tend to mask the sounds of interest. Acoustically treating the tunnel to measure broadband noise in this environment can be especially difficult. However, for high-speed model rotor tests where the problem of interest is impulsive noise (i.e., where the amplitude and frequency content of the acoustic signal are quite high), treating the Ames 7- by 10-Foot Wind Tunnel is a manageable task. Scaling the rotor rotational rate up by a factor of 7, to match the governing nondimensional parameters, also helps by further increasing the frequency of the noise.

As shown in Figure 3, the entire test section of the Ames 7- by 10-Foot Wind Tunnel was lined with a thickness of 3 inches with "Scottfelt." This polyurethane foam, known for its excellent high-frequency absorption characteristics, was installed in open-faced pans.

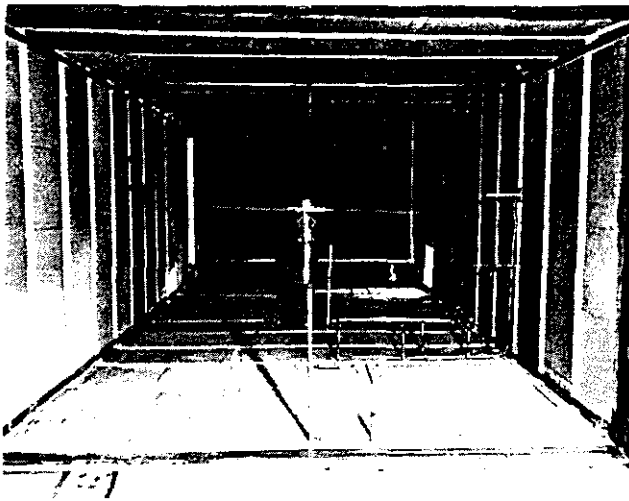


Figure 3. Acoustically treated 7- by 10-foot wind tunnel (with microphones).

An array of Brüel and Kjaer 1/2-inch condenser microphones mounted on aerodynamically shaped struts was used to record all acoustic data. To minimize wind noise, Brüel and Kjaer "nose cones" were used and the microphones aligned to face the relative wind.

Preliminary tests involving the firing of small powder charges indicated that impulsive noise could be measured in the test section with a minimum of interference from local wall reflections. Reverberation from tunnel turning vanes was down at least 12 dB. Although not an acoustically optimum wind tunnel, the simple foam lining permitted adequate measurements of rotor impulsive noise to be taken under a variety of test conditions.

Acoustic data were monitored on an oscilloscope and recorded on a Honeywell (5600) 14-channel FM tape recorder (DC to 10,000-Hz frequency response). Microphone preamplifier gains ( $\pm 20$ -dB range) were determined on-line to maximize signal-to-noise ratios and to avoid peak pressure saturation before the blade slap signal was recorded. Microphone calibration signals were provided by a Brüel and Kjaer portable pistonphone. A one-per-rev signal, magnetically generated by a contactor on the rotor shaft, was also recorded on the FM tape. The data were analyzed on a digital time-series analyzer.

On-line processing of the wind tunnel and rotor operating conditions enabled the operator to iteratively match all four governing nondimensional variables ( $M_H$ ,  $\mu$ ,  $C_T$ ,  $\alpha_{Tpp}$ ). Blade flapping was measured on the rotor, retrieved through sliprings, and summed with shaft tilt to ascertain the rotor tip-path-plane angle.

##### 5. Model/Full-Scale Comparisons

The most direct method for comparing model with full-scale acoustic data is through an analysis of acoustic pressure time histories. Such a comparison is illustrated in Figure 4. In this figure, uncorrected acoustic data, measured in both the model and full-scale test programs, are presented for a low- and a high-advance-ratio condition, in order to illustrate waveform character changes and the relative degree of scaling of the high-speed impulsive noise. The pressure time histories in Figure 4, and in subsequent figures in this paper, were measured at a location directly in front of the rotor and nearly in the plane of the rotor tips, where the most intense signature is known to exist.<sup>9</sup> For each comparison of model to full-scale acoustic data, the rotor test (performance) conditions and the microphone-to-rotor scaled orientation were matched as closely as possible. However, due to both full-scale and wind-tunnel testing constraints, some differences did occur. The particular test conditions, therefore, are referenced below each waveform in Figure 4. In general, scaled microphone-to-hub separation distances were greater in the flight test of Reference 9 than in the scaled model test.

The dominant feature of both model and full-scale waveforms shown in Figure 4 is the similarity in character. At the low-advance-ratio conditions ( $\mu = 0.179$  to  $0.183$ ), shown in the upper half of Figure 4, large negative and almost symmetrical triangular pressure pulses dominate the waveform character. Smaller amplitude positive pressure disturbances precede each negative pressure rise and can be attributed to blade-tip vortex interactions.<sup>9</sup>

Good correlation is also indicated between model and full-scale waveforms at the high-advance-ratio conditions ( $\mu = 0.255$  to  $0.265$ ) shown in the lower half of Figure 4. The negative pressure pulses, which were triangular at the lower advance ratio, become "sawtooth" in character at this high-advance-ratio condition; i.e., the steadily growing negative pressure peak is followed by an impulsive rise in pressure. This sudden change in the acoustic pressure (documented by schlieren photography later in this paper) is traced to a strong discontinuous pressure disturbance that radiates from the advancing rotor blade.

At this high advance ratio, the positive pressure pulses associated with blade-vortex interaction were notably absent in the model rotor data. A range of model tip-path-plane angle variations were investigated, but failed to correlate with full-scale data under similar conditions. This finding suggests that blade-vortex interaction noise may be dependent upon Reynolds number.

As stated previously, high-speed impulsive noise is believed to be strongly dependent upon compressibility. A second comparison of model and full-scale data may be made, therefore, in terms of the compressibility parameter — advancing tip Mach number ( $M_{AT}$ ) — as shown in Figure 5. Here, model data are illustrated by the solid line, and full-scale data from Reference 9 are illustrated by the

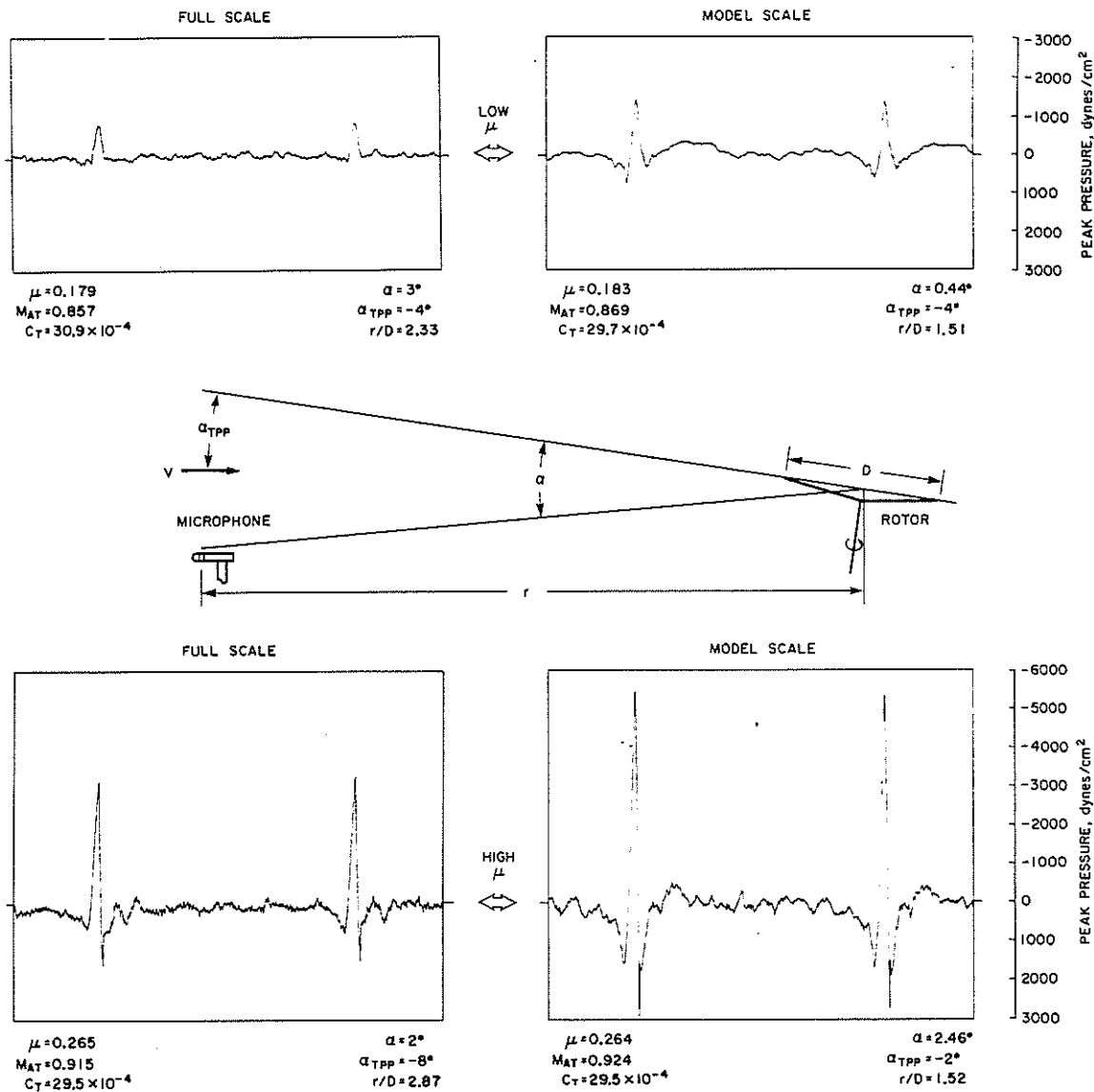


Figure 4. Comparison of uncorrected wind-tunnel and flight-test data for two advance ratios.

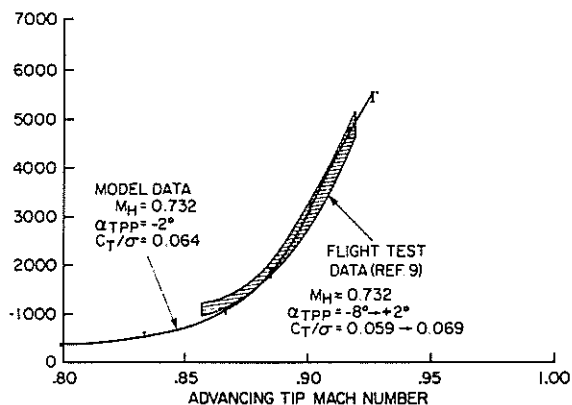


Figure 5. Peak pressure vs advancing tip Mach number - flight-test and wind-tunnel data.

shows that, for high-speed impulsive noise, advancing tip Mach number is the dominant parameter. Small changes can occur in advance ratio without significantly altering in-plane acoustic radiation, if advancing tip Mach number is held constant. To helicopter designers, this means that small reductions in

shaded area. The full-scale data have been corrected for differences in atmospheric density and microphone-to-hub separation distances (using a  $1/r^{0.5}$  law) as explained in Appendix B. Figure 5 indicates good agreement between full-scale and model-scale peak pressure levels when plotted vs advancing tip Mach number. It is shown below that  $M_{AT}$  is, in fact, a first-order nondimensional scaling variable of high-speed impulsive noise.

#### 6. Model Parameter Trends

The rapid increase in magnitude of the negative pressure pulse with increasing advancing tip Mach number is reemphasized in Figure 6. The solid curve (from Figure 5) was obtained at varying advance ratios (0.091 to 0.264), and the dashed curve was obtained at a constant advance ratio (0.229). The similarity of the two curves over a range of advancing tip Mach numbers (0.87 to 0.93)

hover-tip speed or forward speed will significantly reduce impulsive noise through reductions in  $M_{AT}$ , but not through reductions in  $\mu$ .

As illustrated in Figure 6, near  $M_{AT} = 0.8$ , there is a notable difference in acoustic intensity for the constant and varying advance-ratio cases. This difference is undoubtedly related to the radiation efficiency of steady and unsteady acoustic source mechanisms. At relatively high hover tip Mach numbers,  $M_H = 0.73$ , and low advance ratios,  $\mu = 0.09$ , each rotor blade experiences only small variations in the local Mach number around the azimuth implying that the steady compressible source mechanisms are the most likely radiators of far-field acoustic energy. At the same  $M_{AT}$ , but, at the lower hover tip Mach numbers ( $M_H = 0.65$ ) and the higher advance ratios ( $\mu = 0.229$ ), significant variations in the rotor blade local Mach number occur and can be expected to exert more influence on the radiated acoustic field. In this case, unsteady acoustic source mechanisms become more pronounced. The data shown in Figure 6 indicate that the steady radiators of acoustic energy are more efficient generators of impulsive noise than the unsteady ones for similar advancing tip Mach numbers.

This result reinforces the age-old design recipe which is guaranteed to help minimize the noise of rotating devices - ensure operation at low tip speeds. By lowering advancing tip Mach number, the helicopter designer obtains a significant reduction in high-speed noise. Additional reductions are obtained through a decrease in steady compressible noise sources, which are more efficient than unsteady sources as radiators of high-speed impulsive noise.

A small decrease in the absolute amplitude of peak pressure level with increasing tip-path-plane angles is shown in Figure 7. During the acoustic wind-tunnel tests, a change in tip-path-plane angle ( $\alpha_{TPP}$ ) also resulted in an equal change in the angle between the rotor's tip-path-plane and the line connecting the rotor's tip-path-plane and the rotor hub ( $\alpha$ ). Thus, by using this curve, it is impossible to separate these two effects. All that can be said is that, for small increases in  $\alpha_{TPP}$  which result in equal increases in  $\alpha$ , the absolute value of the peak pressure decreases slightly - but not enough to rank the total effect as a primary high-speed impulsive noise parameter.

Figure 8 presents the variation of peak pressure level with changes in thrust coefficient for a microphone positioned nearly in-plane with the plane of the rotor. The data indicate a remarkable insensitivity of impulsive noise to changes in thrust. Notice that the small variations about the mean line of zero slope are caused by variations in tip Mach number about  $M_{AT} = 0.90$ . These variations can be reduced by utilizing Figure 6 to determine peak amplitude corrections between the given tip Mach number and a tip Mach number of 0.90, and then by adding this to the value in Figure 8.

The fact that in-plane impulsive noise is not a function of thrust (i.e., drag), even though the advancing blade is operating past the drag divergence boundary, implies that high-speed impulsive noise is not directly related to the drag divergence phenomena. This has at least one important design implication. The familiar  $C_D$  vs  $M$  curves, at fixed local  $C_L$ , do not have a primary influence on in-plane impulsive noise at high forward speed.

In the detailed comparison of model to full-scale acoustic waveforms, it was observed that the character of the noise changed as the advance ratio increased. A graphic illustration of these events is shown in Figure 9, together with a plot of the peak pressure vs advancing tip Mach number ( $M_H$  is constant and  $\mu$  is varying). In case A

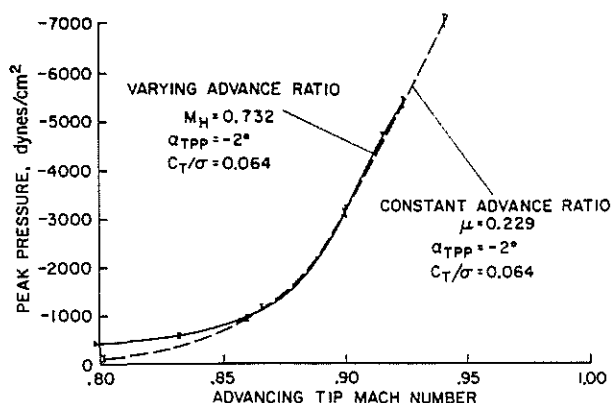


Figure 6. Peak pressure vs advancing tip Mach number - wind-tunnel data.

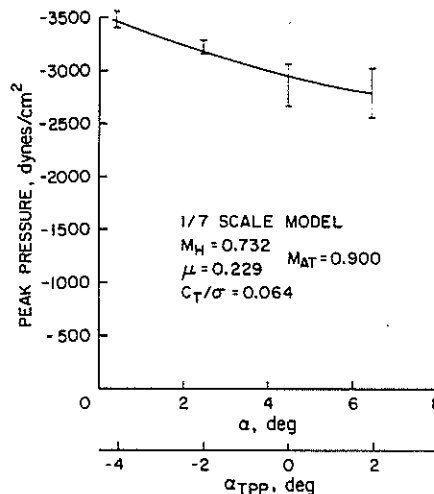


Figure 7. Peak pressure vs orientation angle.

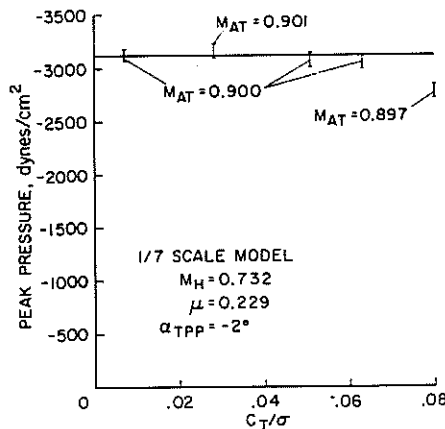


Figure 8. Peak pressure vs changes in thrust coefficient.

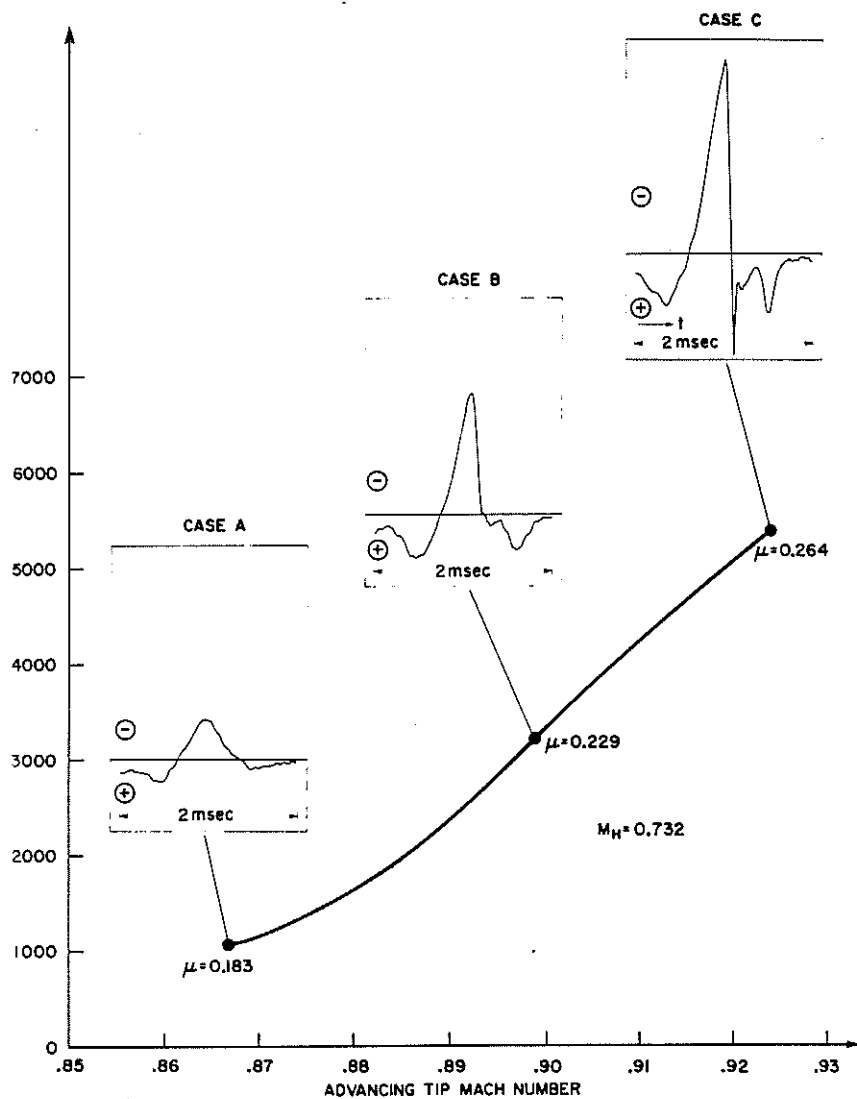


Figure 9. Waveform shape vs advancing tip Mach number.

( $M_{AT} = 0.867$ ), a near symmetrical pulse is observed; the subjective qualities could be described as a loud thumping. As the advancing tip Mach number is increased, the symmetrical pulse becomes "saw-tooth" in character (Case B,  $M_{AT} = 0.90$ ); the waveform consists of a large decrease in pressure followed by an extremely sharp increase in pressure ( $\Delta P/\Delta t = 4 \times 10^6$  dynes/cm<sup>2</sup>/sec). Crispness (many harmonics) and intensity of the acoustic signature are its dominant features. At still higher advancing tip Mach numbers (Case C,  $M_{AT} = 0.925$ ), the peak negative pressure becomes very large, while the sudden rise in pressure becomes nearly instantaneous ( $\Delta P/\Delta t = 10^7$  dynes/cm<sup>2</sup>/sec). Some overshoot can be seen - part of which is real and part of which is due to instrumentation bandwidth limitations. The noise generated by this latter waveform is rich in higher harmonics and can be subjectively classified as harsh and extremely intense.

It was the hypothesis in Reference 9, based upon acoustic measurements, that the rapid increase in pressure (Case C) is due to an unsteady radiating shock wave. Early indications of its formation can be seen in Case B at the lower advancing tip Mach number. Unfortunately, reported theoretical efforts seemed to discount this possibility, because the advancing tip Mach number (the criteria of Reference 6) is still much less than one, even in Case C. Aerodynamicists would be sure to point out that local shocks over the airfoil are present; however, they should be locally fixed to the airfoil and should not radiate to the acoustic far field.

Recently, some newer thoughts on the subject of radiating shocks in unsteady transonic flow have appeared in the literature. Caradonna,<sup>11</sup> utilizing numerical methods, has shown that a shock can move off leading edge of a two-dimensional lifting airfoil in unsteady subsonic flow and radiate into the far field. The experimental work of Reference 12 also indicates that radiating shocks can be present in a steady two-dimensional flow, if the localized lift is varied in an unsteady manner.

Simple geometrical constructions can be used to generate qualitative arguments for the general increase in peak pressure level with increasing advancing tip Mach number. It could be argued that a shock or a strong compression wave is a natural development of this process. Consider only the in-plane acoustic radiation from a pulsating source located at the rotor's tip. At fixed intervals of time, distinct pulses are emitted at the position of the rotor tip and allowed to propagate at the speed of sound in the moving medium (air). For Case C in Figure 9, a top view of the resulting geometric pattern is given in Figure 10. In the direction of forward flight, these simulated acoustic waves bunch together in a process that tends to collect and amplify disturbances around the rotor's disc. Acoustic energy, added over relatively long time intervals, is "skrunched" into a short time interval with a corresponding increase in acoustic intensity. This simple physical process makes the acoustic radiation field "compact," which causes local shape parameters and small disturbances to be emphasized at near transonic speeds. Thus, it is not too implausible to expect this local intensifying process to eventually help generate a radiated compression wave. However, contrary to References 11 and 12, this pressure is periodically shed as a well-defined wave from the rotor's tip.

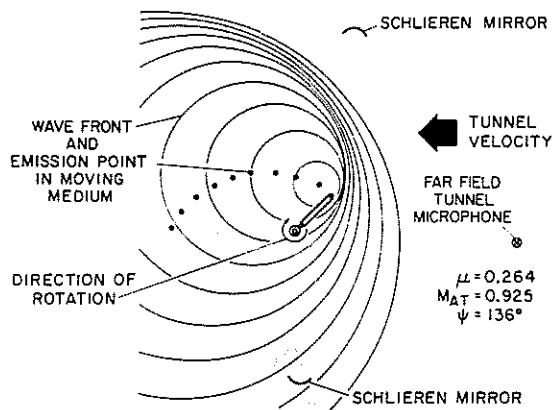


Figure 10. Geometric pattern of high-speed impulsive noise.

To confirm the existence of this radiating shock wave in the rotor's three-dimensional skewed flow environment, a high-speed schlieren system was developed. A general description of the test equipment is given in Appendix C. Figure 11 presents a simple schematic that illustrates the set-up. Schlieren photographs were taken in the plane of the rotor for those conditions which were thought to generate shocks. The angle  $\psi$  describes the azimuthal variation of the advancing rotor.

It should be remembered that these schlieren photographs are two-dimensional pictures of a three-dimensional event. In the photographs which follow, it is difficult to determine where, along the rotor span, the local shocks are positioned.

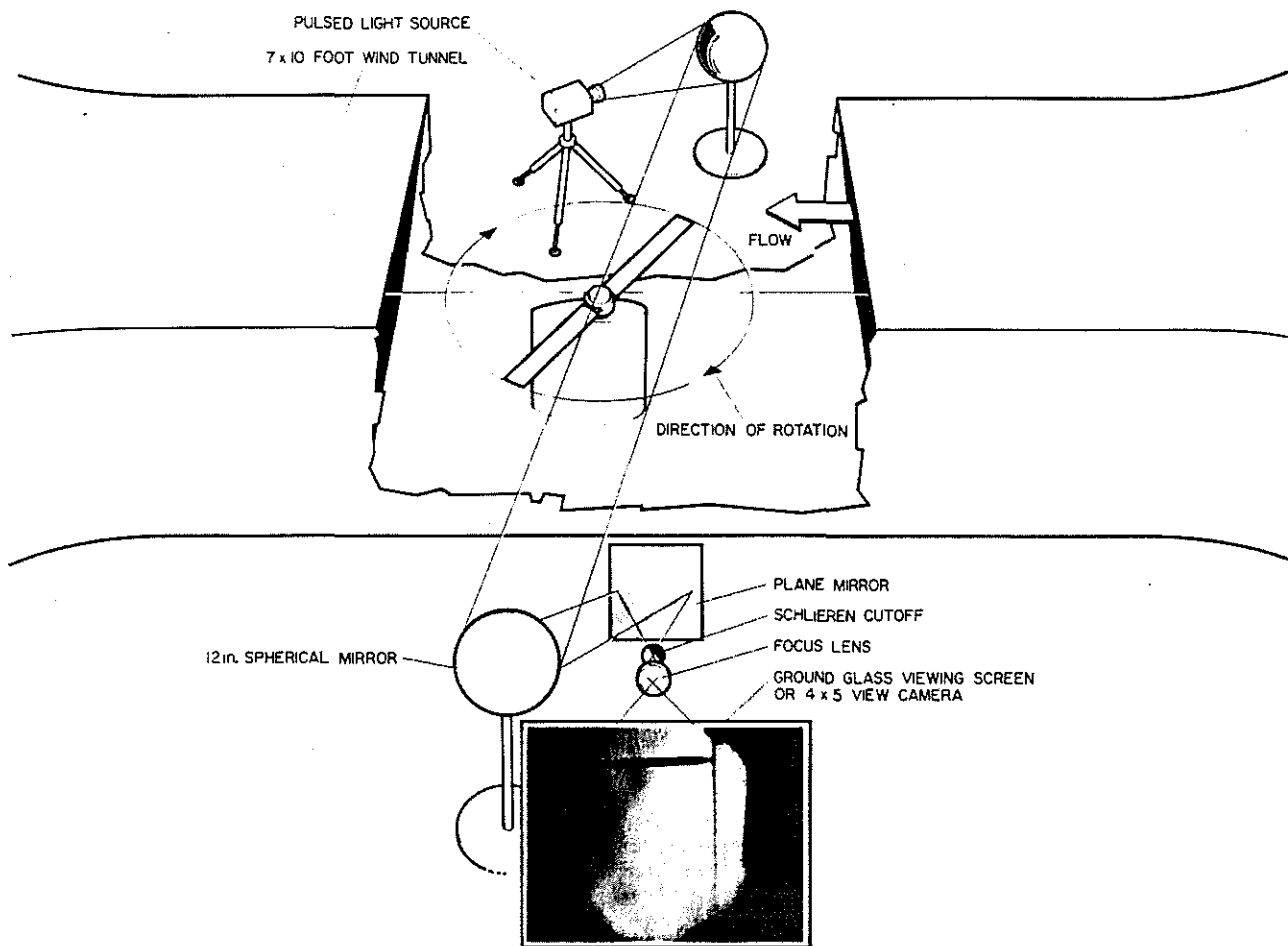


Figure 11. Wind-tunnel/schlieren set-up.

## 7. Schlieren Photographs

When the advancing blade of the model rotor is positioned at  $\psi \approx 135^\circ$ , schlieren photographs show a radiating pressure discontinuity at high advancing tip Mach numbers. Figure 12 presents high-speed pictures of the local three-dimensional flow field near the tip of the rotor blade for the conditions highlighted in Figure 9. At the low advancing tip Mach number (Case A,  $M_{AT} \approx 0.80$ ), no apparent density gradients are detected by the schlieren. This finding implies that there are no strong radiating pressure discontinuities in the flow field and this is confirmed by the shape of the acoustic waveform given in Figure 9, Case A.

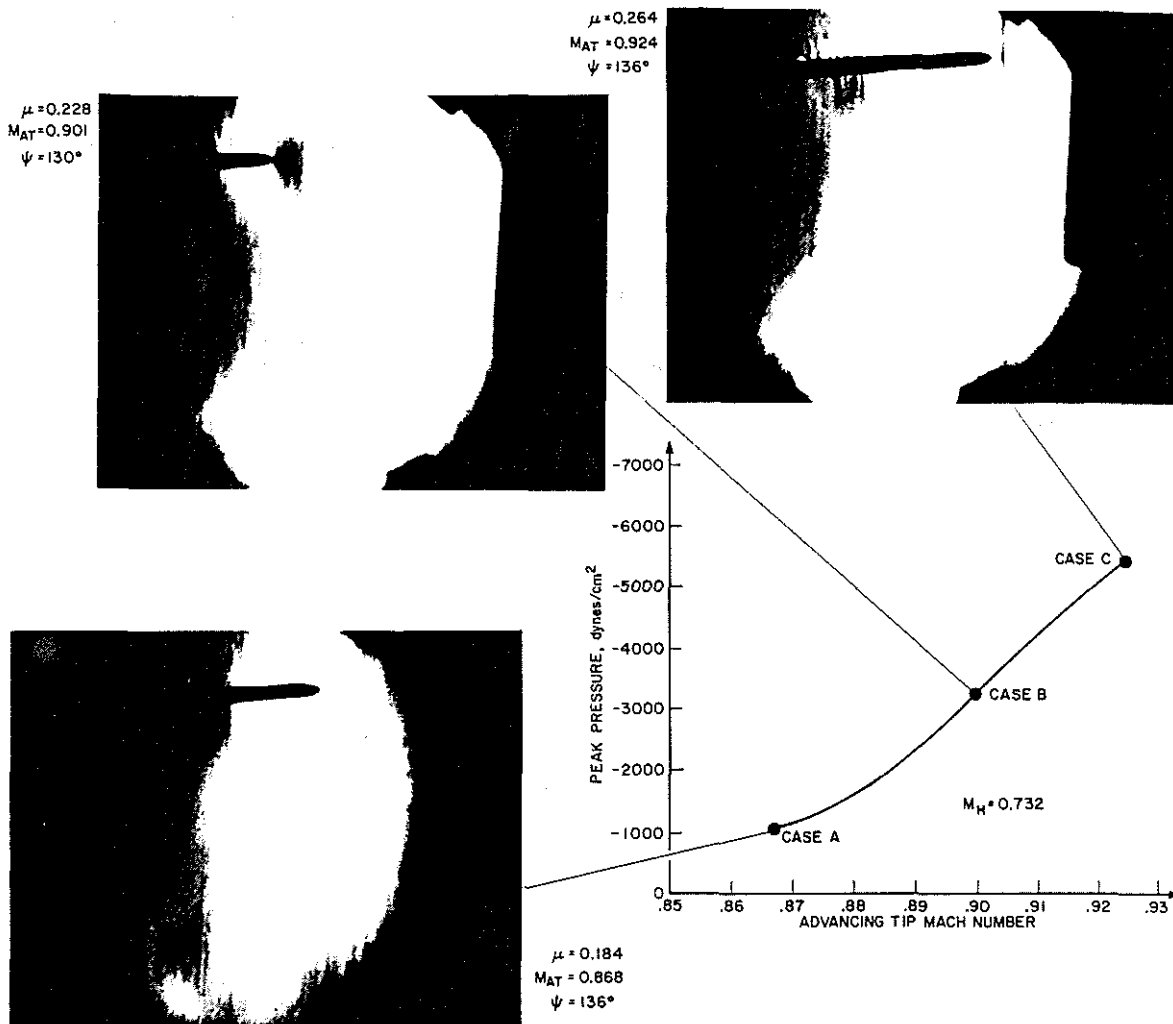


Figure 12. Schlieren image vs advancing tip Mach number

Near  $M_{AT} \approx 0.90$  (Case B), the beginnings of a weak radiating pressure discontinuity can be seen. At this given azimuthal position, the weak discontinuity (shock) is positioned ahead of the leading edge of the rotor as depicted in Figure 12. Thus, as  $\Psi$  is increased (time increased), the shock wave will move further ahead of the model rotor and propagate to the acoustic far field. As indicated in Reference 9, the acoustic radiation will be highly directional, since it is very intense in the direction of the helicopter's forward flight and very near to the rotor's tip-path-plane. Case B of Figure 9 (acoustically) confirms the discovery of a radiating shock through measurement of a sudden rise in acoustic pressure, as previously discussed.

In the high advancing tip Mach number Case C ( $M_{AT} \approx 0.925$ ), the photographic evidence of a radiating shock wave is striking. The sharpness of the wavefront suggests that a fairly strong rise in pressure occurs as the shock traverses a fixed position in space. Once again, this result is confirmed by the in-tunnel, upstream, acoustic pressure time history for Case C in Figure 9.

Figure 13 shows the interesting birth of this shock (Case C). Unfortunately, because tunnel constraints did not always allow the most opportune placement of the schlieren mirrors, some discontinuities appeared in the photographic sequence. For example, the photograph at  $\Psi \approx 85^\circ$  was taken after the schlieren system was moved to optimize the viewing angle. Therefore, the schlieren intensity setting of the  $\Psi = 85^\circ$  photograph does not precisely compare with the other three azimuthal rotor positions. The remaining three photographs were taken with identical schlieren intensity settings, with the rotor shaft tilted fore and aft to change the azimuthal position of the rotor as seen in the schlieren viewing screen. As changed the tip-path-plane angle ( $\alpha_{TPP}$ ) of the rotor with respect to the flow. Fortunately, small variations in  $\alpha_{TPP}$  have already been shown to have a second-order effect on the radiating acoustic signature (Figure 7). In spite of these instrumentation limitations, some important clues about the origin of the radiating shock can be deduced.

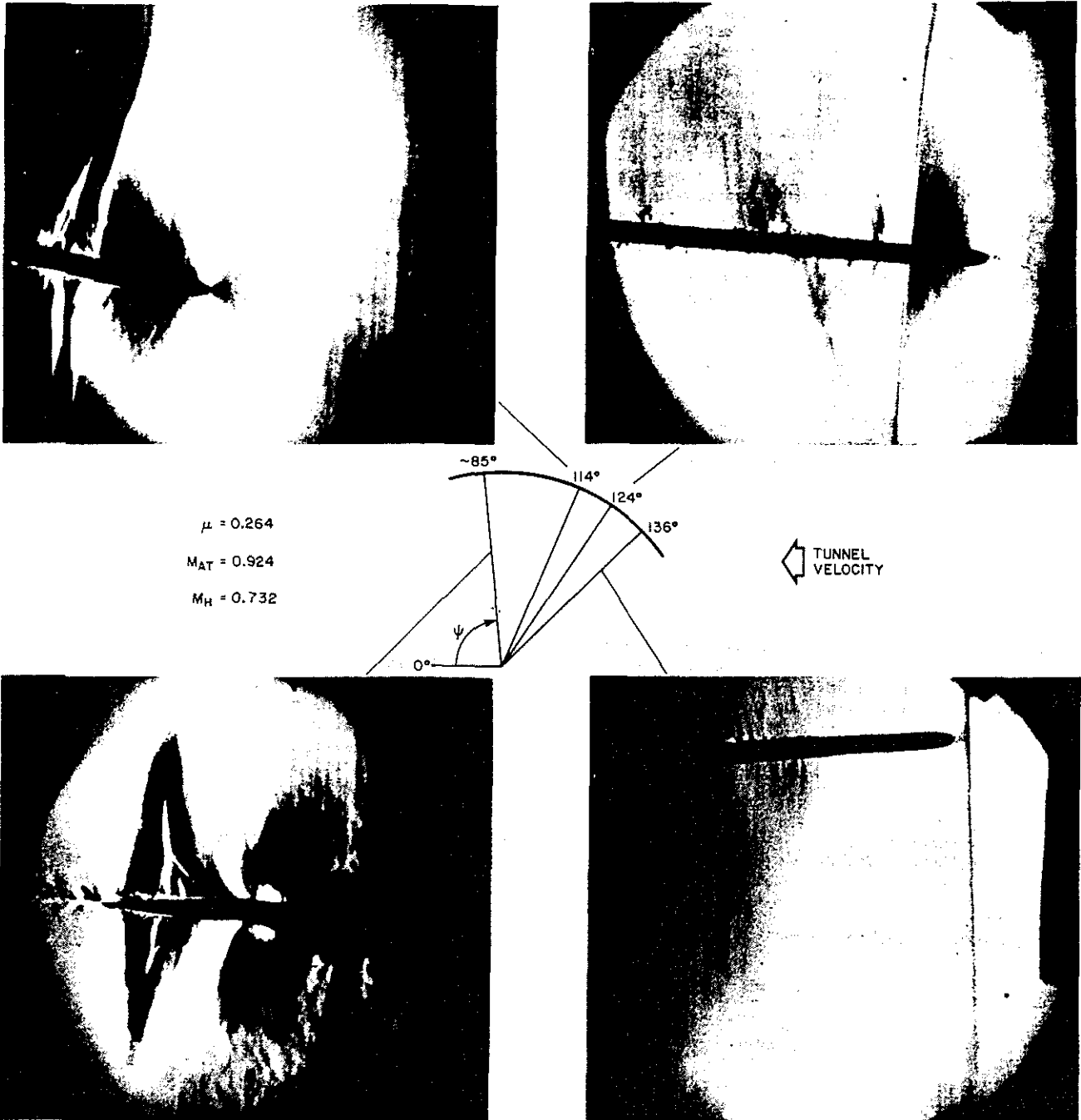


Figure 13. Development of pressure discontinuity (shock).

Part (a) of Figure 13 depicts the local flow field of the advancing rotor blade at an azimuthal position of approximately  $85^\circ$ . Strong three-dimensional shocks are apparent on the upper and lower surfaces of the blade; these shocks react with the boundary layer, thereby causing extensive flow separation. Part of this separation can be shown experimentally to be Reynolds number dependent, which gives some logical reason for the small discrepancy between the full-scale/model-scale peak acoustic pressure levels shown in Figure 5. At this azimuthal position, the shock pattern is what one might have expected from two-dimensional considerations — strong shocks interacting with a laminar boundary layer.

At  $\psi = 114^\circ$ , the local flow field appears to change significantly. The laminar shocks are joined by a large and continuous shock wave. Its continuity through the plane of the rotor suggests that it is not influenced by the local flow field over the blade, but exists beyond the tip of the advancing rotor (as indicated in the propagating wave of Figure 10).

As the rotor advances to the  $\psi = 124^\circ$  position, the laminar shocks appear to weaken, while the large continuous shock seems to intensify and move forward with respect to the leading edge of the airfoil. Finally, at an azimuthal position of  $\psi = 136^\circ$ , the strong pressure discontinuity moves ahead of the airfoil into the oncoming flow, and thus radiates to the acoustic far field.

## 5. Concluding Remarks

The mysteries of high-speed helicopter impulsive noise are beginning to unfold as new and improved data gathering techniques are perfected. The in-flight method of measuring noise with a "flying" microphone probe has defined the true character of helicopter impulsive noise. A conventional hard-walled wind tunnel, with appropriate acoustic treatment and instrumentation, has been shown to be an effective method of measuring these same high-speed noise characteristics from model rotors. A detailed comparison between the acoustic waveforms and peak pressure amplitudes from both testing techniques has demonstrated that the data scale remarkably well, opening the way for future acoustic wind tunnel experiments.

Advancing tip Mach number and advance ratio have been shown to be first-order high-speed impulsive noise parameters, the former being the most important for the UH-1H helicopter. Variations in tip-path-lane angle cause second-order changes in the peak in-plane acoustic pressure, while changes in thrust cause no measurable differences.

The propagation of the resulting intense pressure pulse was discovered to decay less rapidly than point source model at comparable measurement distances. The geometrical characteristics of the locally generated sound waves are believed to be responsible for this slow decay.

The waveform of high-speed impulsive rotor noise changes character as the advancing tip Mach number is increased. At  $M_{AT} = 0.85$ , a large near-triangular negative pressure pulse is observed. At  $M_{AT} = 0.90$ , the pulse becomes larger in magnitude and "sawtooth" in character; the return to near atmospheric pressure from the large negative value is "step-like" in character. This rapid increase in pressure has been correlated with the formation of a weak, radiating shock wave. At  $M_{AT} = 0.925$ , the "sawtooth" acoustic waveform becomes larger in amplitude and exhibits an almost discontinuous increase in pressure from the large negative value. This rapid increase in acoustic pressure correlates with the periodic radiation of a shock wave from the advancing side of the rotor. Although the detailed formation mechanisms are unknown, a continuous shock develops off the tip of the airfoil between  $\psi = 85^\circ$  and  $110^\circ$ . As  $\psi$  increases, the shock moves forward ahead of the leading edge of the airfoil and propagates in the direction of forward flight.

Developing a better understanding of the compressible flow environment and its relation to radiated noise is a fascinating subject for future experimental and theoretical research. From our own work, the strength or position of the radiating shock wave does not appear to be thrust or Reynolds number dependent. The main unanswered questions are: What causes the formation and governs the ultimate strength of this large radiating shock? Do the local flow shocks coalesce off the tip of the airfoil into one large pressure discontinuity, or does the under-expansion of the acoustic pressure due to thickness effects become so great that the resulting increase in pressure which follows is not isentropic? As in all basic research, although we have isolated a key acoustic mechanism and solved some of the unknowns of high-speed impulsive noise, it appears that we have only begun to understand the detailed complexities of the problem.

## 6. Acknowledgement

The authors are indebted to Mr. Larry D. Russell for his technical guidance and assistance in designing and setting up the schlieren system, and to Mr. Elwood R. Leibfritz for his ingenuity and craftsmanship in fabricating the model rotor blades.

## APPENDIX A

### 0. Comparison of Test Parameters

PARAMETER	SYMBOL	APPROXIMATE RANGE OF VALUES TESTED	
		IN-FLIGHT TEST (REF 9)	WIND TUNNEL TEST (PHASE I)
HOVER TIP MACH NUMBER	$M_H$	0.73	0.6 $\rightarrow$ 0.76
ADVANCING TIP MACH NUMBER	$M_{AT}$	0.86 $\rightarrow$ 0.92	0.73 $\rightarrow$ 0.93
ADVANCE RATIO	$\mu$	0.17 $\rightarrow$ 0.27	0.18 $\rightarrow$ 0.27
THRUST COEFFICIENT	$C_T$	$26 \times 10^{-4} \rightarrow 32 \times 10^{-4}$	0 $\rightarrow 44 \times 10^{-4}$
TIP PATH PLANE ANGLE	$\alpha_{TPP}$	$-8^\circ \rightarrow +6^\circ$	$-6^\circ \rightarrow +4^\circ$
ROTOR SOLIDITY	$\sigma$	0.0464	0.0464
REYNOLDS NUMBER (BASED UPON BLADE CHORD)	RN	$9 \times 10^6$	$1.3 \times 10^6$
ROTOR DIAMETER	D	48 ft	6.85 ft
ROTATIONAL RATE	$\Omega$	5.4 cycles/sec	30 cycles/sec $\rightarrow$ 39 cycles/sec

APPENDIX B

11. Acoustic Data Scaling

The acoustic pressure that results from aerodynamic noise sources can be shown to be a linear function of atmospheric density ( $\rho$ ) if thrust coefficient ( $C_T$ ) is held constant. Therefore, when full-scale acoustic data taken at altitude are compared with model-scale data recorded near sea level, an amplitude correction is required. In this paper, the peak negative pressure amplitude of the flight test data has been corrected to model test atmospheric conditions by the relation:

$$\text{Flight test acoustic pressure corrected for density} = \left( \text{Flight test acoustic pressure} \right) \times \left( \frac{\rho_{\text{model}}}{\rho_{\text{flight test}}} \right) \quad (\text{B-1})$$

As discussed in the text, all four nondimensional aerodynamic performance variables as well as geometrical scaling relationships constitute a sufficient condition for a valid comparison.

Geometric acoustic scaling of microphone-to-hub separation distances follows readily from a dimensional analysis of the governing acoustic equations (see, for example, Reference 13). Model acoustic data should be compared with full-scale acoustic data at scaled microphone-to-hub separation distances, ( $r/D$ ), measured in rotor diameters. Unfortunately, tunnel constraints and changing flight-test microphone-to-hub separation distances often prohibited exact matching of these scaled distances, thus requiring that a suitable correction be applied to either set of data. For convenience, the full-scale data of Reference 9 have been corrected to the fixed microphone-to-model hub distance of  $r/D = 1.52$ .

If the microphone is assumed to be in the acoustic and geometric far field of the rotor, then the acoustic intensity is known to be inversely proportional to  $r/D$ . Therefore, full-scale acoustic amplitudes can be corrected to model scale by Equation B-2 with  $n = 1$ .

$$\text{Flight test acoustic pressure corrected to } (r/D)_{\text{model}} = \left[ \text{Flight test acoustic pressure} \right] \times \left[ \frac{(r/D)_{\text{full scale}}}{(r/D)_{\text{model}}} \right]^n \quad (\text{B-2})$$

The entire matrix of test points of Figure 5, Reference 9, were corrected to  $(r/D)_{\text{model}} = 1.52$  with  $n = 1$  as shown in Figure B-1 by the lightly shaded region. Accurate flight test separation distances were calculated by utilizing the differences in arrival times between the 1/rev signal transmitted over the radio channel and the impulsive acoustic signal recorded by the microphone. Fair agreement with model test data is indicated.

From theoretical considerations, it can be argued that the microphone was not stationed in the acoustic and/or geometric far field in either test. The pressure wave which is radiated at high advancing tip Mach numbers is geometrically large and its propagation is not governed by point-source radiation arguments near the plane of rotation at small  $r/D$ . This implies that measured peak pressures will be inversely proportional to some fractional power of  $r/D$  at small  $r/D$ , with the fraction increasing to 1 with increasing  $r/D$  and decreasing  $M_{AT}$ .

A few specialized conditions were included in the Reference 9 test program to evaluate the acoustic pressure's dependence on radiation distance. These resulting measurements indicated that the exponent of Equation B-2 is definitely less than 1 at  $r/D$  between 1.5 and 2.6, and is a function of advancing tip Mach number, advance ratio, or both. An average value of  $n \approx 0.5$  was chosen to be representative of the few measured points which were available.

By using  $n = 0.5$  in Equation B-2, the data reported in Figure 5, Reference 9, can be collapsed into the darkened region shown in Figure B-1. Good agreement with model acoustic data taken in the wind tunnel is now apparent.

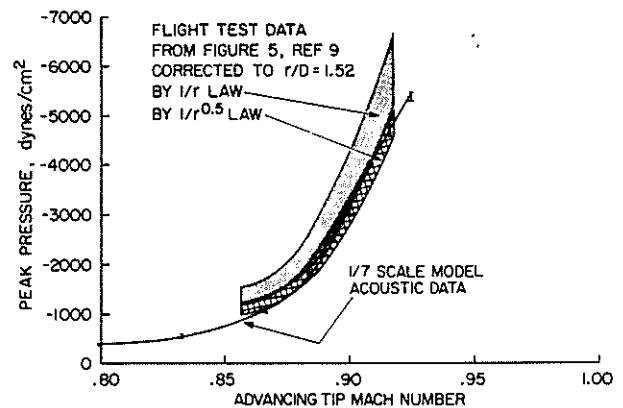


Figure B-1. Flight-test data corrected for  $1/r$  and  $1/r^{0.5}$ .

## APPENDIX C

### Strobed Schlieren System

The schlieren system, shown in Figure 11, used in the wind-tunnel test, consisted of two 12-inch diameter, 60-inch focal length spherical mirrors; a model 1531-AB externally triggered STROBOTAC for a light source, and a standard 4 x 5-inch view camera as viewing screen and film holder. The time delay feature of the STROBOTAC allowed for a smooth, continuous time (angle) change in firing, thus permitting viewing at various azimuthal angles - within limits of the mirrors and the physical constraints of the model. The repetitious firing of the strobe permitted "real-time" viewing of the rotor at any given angle or position. A single-fire mode was found best for recording pictures. Very little distortion was observed in the image, even though space considerations required the system to be folded.

It should be noted that this system is not a true schlieren system. Normally, a point light source is used; but, to increase the light output, a line source, oriented vertically, was used in this test. In place of the conventional knife edge, two narrow brass ribbons (approximately 1 mm wide and separated approximately 0.1 mm) were used. The light source image was focused on the slit between the two-ribbons with the effect being that light areas in the image were caused either by rays passing through the slit between the ribbons (the undeflected background) or by rays passing around the ribbons (the very highly deflected shock waves). Dark areas in the image were caused by rays striking the ribbons (the moderately deflected gradients) on either side of the slit.

Such a system has two main advantages or disadvantages, depending upon one's point of view. First, light gradients normal to the line source were observable. Second, nearly all quantitative information is lost, but with a significant increase in the qualitative and the overall sensitivity of the system (because of the much brighter source). It must be realized that no distinction can be made as to whether a given object passed through a positive gradient or a negative gradient (the cutoff is symmetrical), only whether deflection was large or small.

### References

- W. F. Hilton, The Photography of Airscrew Sound Waves. Proceedings of the Royal Society, Series A-169, 174-190 (1939).
- L. Gutin, On the Sound Field of a Rotary Propeller. NACA TM 1195 (1948).
- D. E. Ordway, An Aerodynamic Theory of a Supersonic Propeller. OSR TN-56-297, ASTIA Number AD 89498. Cornell University (June 1956).
- H. H. Hubbard and L. W. Lassiter, Sound from a Two-Bladed Propeller at Supersonic Tip Speeds, NACA Report 1079 (1952).
- D. L. Hawkins and M. V. Lowson, Theory of Open Supersonic Rotor Noise. Journal of Sound and Vibration, 36, No. 1, 1-20 (Sept. 1974).
- M. V. Lowson and R. J. Jupe, Wave Forms for a Supersonic Rotor. Journal of Sound and Vibration, 37, No. 4, 475-490 (Dec. 1974).
- F. Farassat, Theory of Noise Generation from Moving Bodies with an Application to Helicopter Rotors, NASA TR R-451 (Dec. 1975).
- Richard H. Lyon, Radiation of Sound by Airfoils that Accelerate Near the Speed of Sound. Journal of the Acoustical Society of America, 49, No. 3, Part 2, 894-905 (March 1971).
- F. H. Schmitz and D. A. Boxwell, In-Flight Far-Field Measurement of Helicopter Impulsive Noise. AHS Paper 1062. Presented at the 32nd Annual National Forum of the American Helicopter Society (May 1976). (Also presented at the First European Rotorcraft and Powered Lift Aircraft Forum, University of Southampton, Southampton, England, Sept. 22-24, 1975.)
- R. A. Arndt and D. A. Boxwell, A State-of-the-Art Report on Aeroacoustic Testing in Conventional Wind Tunnels. Presented at the 84th Meeting of the Acoustical Society of America, Miami Beach, Florida (Nov. 28-Dec. 1, 1972). (Unpublished.)
- F. X. Caradonna and M. P. Isom, Numerical Calculation of Unsteady Transonic Potential Flow over Helicopter Rotor Blades. AIAA Paper 75-168. Presented at AIAA 13th Aerospace Sciences Meeting, Pasadena, California (Jan. 20-22, 1975).
- H. Tijdeman, On the Motion of Shock Waves on an Airfoil with Oscillating Flap in Two-Dimensional Transonic Flow, National Aerospace Laboratory NLR TR 75038. The Netherlands (1975).
- H. Sternfeld et al. An Investigation of Noise Generation on a HOVERING Rotor, Part II. Report D210-10550-1. U. S. Army Research Office (Nov. 1972).